submitted to *Geophys. J. Int.*

Field evidence for non-linear IP effects in a volcanic hydrothermal system using reciprocal data.

L. Vanhooren[1,2⋆], W. Deleersnyder[1], W. Deconinck[1], A. Flores-Orozco[3], F. Nguyen[4], C. Caudron[2], T. Hermans[1]

[1] *Laboratory of Applied Geology and Hydrogeology, Ghent University, Belgium.*

[2] *G-Time laboratory, Université libre de Bruxelles, Belgium.*

[3] *Department of Geodesy and Geoinformation, TU-Wien, Austria.*

[4] *Urban and Environmental Engineering, ULiege, Belgium.*

June 25, 2025

SUMMARY

In electrical geophysical methods it is often assumed that the resistivity or chargeability, behaves linearly with the applied electrical current. However, non-linearity has been reported in Induced Polarization (IP) and can be caused by oxidation-reduction reactions or reactions at the surface of clay minerals. Methods to determine the presence of non-linear effects exist and involve analysis of the harmonic distortion of spectral IP data. Measurement of reciprocal data is standard practice in many ERT surveys in the context of data filtering and error quantification. When assuming a system behaves linearly, the normal and reciprocal measurements should yield the same distribution of values. Consequently, a systematic misfit between the two can indicate non-linearity. Here, we present the case of time domain IP (TDIP) data acquired in a volcanic hydrothermal system (VHS), with a strong discrepancy in both observed data and inversion of normal and reciprocal data, presented as a positive shift of the reciprocal decay curves ($>$100 mV/V). The inversion shows a strong discrepancy in the imaginary part, of 20 mS/m, localized on the southern part of the profile. In the complex environment of a VHS we interpret the observed non-linear IP effect as the result of oxidation-reduction reactions at the interface of iron oxides or sulfides. Our study suggests that analysis of normal-reciprocal misfit can be further used as an interpretation tool for the presence of non-linear effects.

Key words: non linear IP effect – reciprocity – volcanic hydrothermal systems

1 INTRODUCTION

Induced polarization (IP) is a geo-electric method that characterizes the ability of the subsurface to temporarily store electrical charges. IP is usually expressed by the resistivity and chargeability or the by the real and imaginary components of the complex conductivity, with the imaginary component and the chargeability being linearly related (Binley & Slater, 2020). It is sensitive to the presence of (semi-)conductive minerals (Pelton et al., 1978), certain clays (Lévy et al., 2018), and pore-space geometry (Weller et al., 2016). In environments where bulk electrical parameters can be caused by different processes (for example, low resistivity can be caused by clays and/or high salinity), IP can further distinguish between the source of the signals. Hence, IP is often preferred in complex environments over the more traditional pure DC-methods like ERT (Ghorbani et al., 2018; Slater & Lesmes, 2002). The IP method has gained popularity in volcanological studies where it has been successfully applied to identify the presence of conductive minerals such as magnetite and pyrite (e.g. Lévy et al., 2018, 2019; Ghorbani et al., 2018). Identification of fracture networks influencing local flow patterns and therefore the degassing behavior (Troiano et al., 2021), for mapping of the extent of hydrothermal alterations (e.g. Revil et al., 2002; Vanhooren et al., 2025) and has been suggested for detection of CO_2 rich groundwater which can be related to a magmatic origin (Defourny et al., 2020).

It is often assumed for simplicity that the measured parameters exhibit linear behaviour (Pelton et al., 1978), i.e. that electrical properties are independent from the potential difference. This linearity is at the heart of the reciprocity theorem (Parasnis, 1988). However, at low frequencies, typical of time-domain induced polarization (TDIP), non-linear responses can occur (Olhoeft, 1985). Although often neglected, non-linearity can provide valuable information, especially in a hydrother-

⋆ Lore.Vanhooren@UGent.be

mally active environment where the interpretation of IP signals is not always straightforward. The effect can be caused by (1) oxidation-reduction reactions due to the corrosion of (semi-)metallic minerals, such as pyrite or magnetite; (2) the less well understood ion-exchange reactions at the surface of clay minerals and zeolites (Olhoeft, 1979) and; (3) reactions between clays and organic contaminants (Olhoeft, 1985). More recently, a fourth process was proposed by (Hallbauer-Zadorozhnaya et al., 2015, 2016), arguing for membrane polarization to facilitate a non-linear IP effect, supported by a field case where both chargeability and resistivity were dependent on the current density (Hallbauer-Zadorozhnaya et al., 2015). Methods to identify non-linearity are proposed by the aforementioned authors, but often generally require the collection of spectral induced polarization data. However, field deployment of IP is often done in time domain, which is available in most commercially available instruments. To our knowledge Hallbauer-Zadorozhnaya et al. (2016) were the first to develop a methodology applicable to field data; they rely on current density to be an indicator for non-linearity where the measurement of a profile should yield a different resistivity and chargeability distribution under different current densities.

In this study propose an alternative methodology applicable to field data to study non-linear behaviour by relying on the falsification of the reciprocity principle to interpret a non-linear IP signal. The reciprocity theorem states that, in a geo-electric survey, when current and potential dipoles are interchanged, the readings should yield the same result given a homogeneous, source-free and linear character of the subsurface (Parasnis, 1988). The reciprocal is widely used in ERT because of its applicability in noise quantification (Slater et al., 2000). Here we extend the analyses of the reciprocal to identify zones of non-linearity. Note that this approach is in line with the proposition by (Hallbauer-Zadorozhnaya et al., 2016), since reciprocal measurements can be characteristic of various current densities depending on the measurement protocol.

2 MATERIALS AND METHODS

2.1 Complex Conductivity

The complex conductivity (σ^*) is a measure of the electrical properties of the subsurface. It is given by its real (σ') and imaginary (σ'') parts where the real part corresponds to the conduction strength or electromigration properties. The imaginary part represents the temporal, reversible charge storage, or polarization (Binley & Slater, 2020) hence the term induced polarization (IP). The complex conductivity σ^* can also be represented in terms of the magnitude $|\sigma|$ and phase shift φ, referring to the tangent of the real and imaginary components, the complex conductivity can thus be written as:

$$\sigma^* = |\sigma| e^{i\varphi} = \sigma' + i\sigma'' \tag{1}$$

and

$$\sigma' = |\sigma| cos\varphi, \tag{2}$$

$$\sigma'' = |\sigma| sin\varphi. \tag{3}$$

In porous media, in absence of electronic conductors, the conduction is controlled by electrolytic and surface conductivity. The prior is described by Archie's law (Archie, 1941) and is proportional to the fluid conductivity, saturation and pore space geometry, i.e. the total porosity and connectivity of the pore space. While the surface conductivity is controlled by surface charges and area. This effect cannot be neglected in environments rich in fine materials (e.g. clay, silt, graphite), metals or organic materials (Flores-Orozco et al., 2011). Hence Archie's law warrants an extra term and can be generalized as the following (Waxman & Smits, 1968):

$$\sigma_b = \frac{1}{F} S^n (\sigma_w + f(\sigma_w, CEC, S), \tag{4}$$

stating that the bulk conductivity σ_b is a functions of the water conductivity σ_w, the cation exchange capacity (CEC, accounting for the surface charge), the saturation S and the formation factor F.

The presence of polarizable material complicates the interpretation, since the polarization of charge can be controlled by multiple mechanisms. In porous media, the most common one is related to diffusion-controlled polarization in the electrical double layer (EDL) due to the formation of local charge gradients. Two mechanisms drive the creation of such gradients, (1) blockage of ions in pore throats leading to a localized access of ions (membrane polarization); (2) the displacement of counter-ions in the Stern layer at mineral surfaces (Stern layer polarization), which is more abundant in minerals with a large surface area such as clays.

A second polarization type arises from the interaction of metallic minerals with an electrolytic fluid where the strong phase response is the result of a difference in transport rate between the ions (elecrolytic fluid) and electrons (metallic grain). Correlations have been reported between the strength of the phase response or imaginary conductivity and the volume of metallic minerals (Pelton et al., 1978; Slater et al., 2005). Polarization due to metallic minerals characteristically yields larger bulk electrical responses in terms of apparent chargeability or phase shift than EDL processes.

The complex conductivity arising from the aforementioned processes is strongly influenced by the conductivity of the pore fluid. At low salinity, the imaginary conductivity increases with increasing salinity until it reaches a plateau. At very high salinity, a drop in σ'' is reported due to the reduction in ion mobility in the EDL (Lesmes & Frye, 2001; Weller et al., 2015).

2.2 Study Area

The study area is located on the Reykjanes Peninsula, Iceland, which has been volcanically active again since 2021. Based on historical data and recent events, six volcanic systems have been identified (Sæmundsson et al., 2020), not all of them host an active volcano, but can be geothermally active with an old magma intrusion as the heat source. This is the case for our study area, the Reykjanes system, hosting a high-temperature geothermal field of < 1km². Field operator HSOrka commissioned a 100MWe powerplant in 2006 for the production of electricity and warm water (Fridleifsson et al., 2020). Reservoir temperatures reach between 250°C and 300°C at a few 100 meters depth (Fowler et al., 2015) and more than 300°C between 1 and 2.5 km deep (Kadko et al., 2007). Because of the proximity to the ocean, the hydrothermal system is 100 % recharged by seawater (Kadko et al., 2007), which does not exclude the fact that a small ($\approx$30 m) freshwater lens develops due to infiltrating rainwater (Sigurdsson, 1986). Host rocks are young, highly permeable basalts (Björnsson et al., 1970) that exhibit a traditional progressive hydrothermal alteration with depth (Marks et al., 2010).

The electrical conductivity signature of the field has been studied for the exploration of the geothermal system using transient electromagnetic (TEM) and magnetotelluric (MT) soundings

(Karlsdottir et al., 2020), and controlled source electromagnetic (CSEM) measurements (Bretaudeau et al., 2021). Both studies confirm the presence of a low resistivity cap (1-3 Ωm), with an irregular geometry reaching the surface in the hot spring area and dipping down radially towards 1 km depth. The cap is underlain by a high resistivity core (10-100 Ω), characteristic for a geothermal field. High levels of heterogeneity have been reported in the shallow layer (< 200m) (Karlsdottir et al., 2020). A shallow electrical resistivity tomography (ERT) survey, supported by induced polarization (IP), and self-potential (SP) show the types of heterogeneity (Vanhooren et al., 2025). The complexity of the shallow system is reflected by different types of surface manifestations corresponding to different geophysical signals: (1) Areas with intense surface alteration, such as mud pools and high local temperature gradients (6°C/cm), are characterized by a low resistivity signal (< 5 Ohm.m) and a weak normalized chargeability (< 3 mS / m), mainly caused by the presence of clays. (2) Part of the area is characterized by a shallow sealing structure in the upper 10 m, here the resistivity signature is low (<5 Ohm.m) but the normalized chargeability is higher (8-10 mS/m), the presence of the seal impedes movement of geothermal fluids to the surface, as a result no surface alteration is observed. (3) The majority of the site has no visible alteration on the surface or geophysical indications for alteration in the subsurface and are characterized by a high resistivity (< 500 Ohm.m) and the absence of signal in normalized chargeability. However, other geothermal expressions can be possible, such as steam vents, which typically have a positive self potential anomaly caused by upflow of hydrothermal fluids. This highly variable resistivity distribution is controlled by local fracture and fluid flow patterns, where preferential pathways cause more progressive alteration Vanhooren et al., 2025, which is also observed by irregular, localized degassing patterns (Fridriksson et al., 2006).

2.3 Data acquisition and processing

The field site is located in the southwest of Iceland, in the Reykjanes Geothermal area (Fig. 1). The static characterization of the site can be found in Vanhooren et al. (2025). An ERT / IP monitoring profile was installed at a location with highly variable hydrothermal activity. The monitorng profile is 355m long, consisting of 72 stainless steel electrodes, with a spacing of 5m. Measurements are

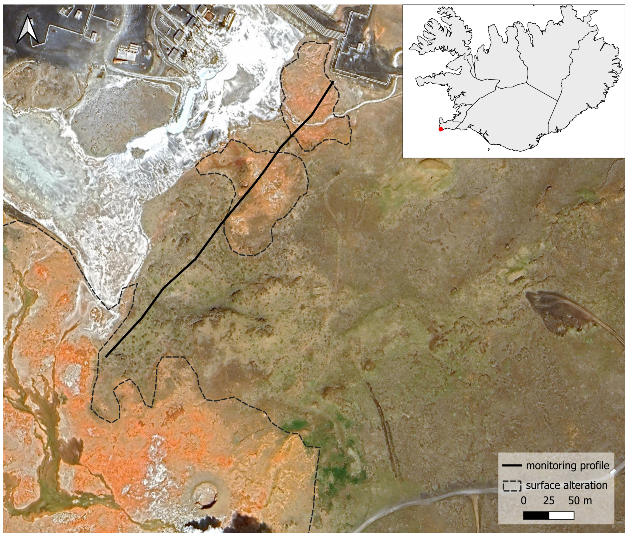

Figure 1. Location of the monitoring profile, the field area is indicated on the map of Iceland by the red dot. The facilities of the powerplant can be seen in the North, the Gunnhuver crater in the South. The body of water West of the profile consists of discharge water from the powerplant.

made using a *Syscal Pro* from IRIS instruments, using the *Syscal Monitoring Unit* to facilitate remote operation for monitoring. A square wave is injected using a 50% duty cycle and a pulse length of 1 s. For the chargeability measurements, after a delay of 40 ms, the voltage is measured in 20 semi-logarithmically ordered windows. The semi-logarithmic scheme was chosen because the time-windows are closer together in the first part of the decay, with a higher signal-to-noise ratio, and spaced further apart with lower S/N. Time windows 1-8 are measured every 20 ms, 9-14 every 40 ms, and 15-20 every 80 ms. Measurements are done using the multi-gradient protocol, with a normal protocol consisting of 1624 quadrupoles, while 2758 are collected in the reciprocal. The extra quadrupoles in the reciprocal are needed in order to make optimal use of the 10-channel system.

Due to the high salinity in the field (Sigurdsson, 1986), we expect a low signal-to-noise ratio for the TDIP data. The normal-reciprocal discrepancy is not suitable for filtering TDIP data based on data quality since it cannot sufficiently identify outliers and readings with poor S/N ratios (Binley & Slater, 2020). More appropriate methods include a detailed analysis of the individual decay curves (e.g. Flores Orozco et al., 2018; Evrard et al., 2018).

Here, we assess the quality of the curves by fitting a decaying exponential function, and calculating the root-mean-square-error (rmse) with the observed data. Curves with an rmse $> 75\%$ are removed from the data. Additionally, curves that asymptotically decay towards a non-zero value are removed (Evrard et al., 2018) as well as non-decaying and negative curves. Note that more advanced methods exist for data filtering, accounting for the spatial variability of the decay curves (Flores Orozco et al., 2018).

Inversion is done using CRTomo (Kemna, 2000), solving the smoothness constrained regularized inversion using a Gauss-Newton itrerative approach in terms of complex resistivity ρ^*, the inverse of σ^*. The calculations are expressed in terms of resistivity amplitude and the phase shift φ eq (1). In order to prepare the data for inversion, the chargeability obtained from TDIP measurement are linearly converted to phase shift in the frequency domain, relying on a constant phase angle response (Kemna, 2000). We chose to visualize the results in terms of complex conductivity with its real and imaginary parts, eqs (2)-(3). The regularized inversion can be further constrained by including prior information in the form of a reference model (Caterina et al., 2014). Care should be taken in the choice of the reference model as it introduces some subjectivity in the inversion (Oldenburg & Li, 1994). Here, we use a homogeneous reference model with a resistivity of 1 Ωm and a phase of 0 mrad. The closeness factor, weighing the importance of each cell (Hermans, 2014), is 0.01.

To determine the non-linear IP effect, the two datasets (normal and reciprocal) are processed independently (i.e. same filtering steps and inversion parameters). In order to appropriately assess the difference between the normal and reciprocal, the additional points are removed from the reciprocal so the two datasets contain the same quadrupoles, where each quadrupole has a reading in the normal and reciprocal. In the presence of a non-linear signal, both the data and inverted models should show a considerable difference between the normal and reciprocal. A discrepancy can also be caused by measurement errors or noisy data. The latter can however be excluded if the discrepancy is consistent through time, as observable in a long monitoring data set.

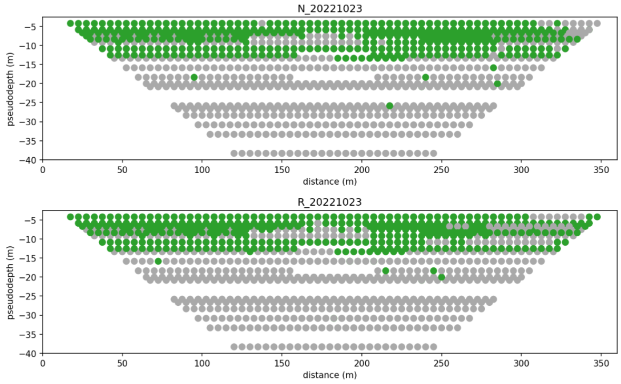

Figure 2. Pseudosections showing the quadrupoles accepted after decay curve analysis for the normal (top) and the reciprocal (bottom) profiles.

3 RESULTS

3.1 Static Processing and Inversion

The decay curve analysis removes 62 % from the normal data set and 63 % from the reciprocal data set. In both cases, almost no data is retained below a pseudodepth of 15 m (Fig. 2). This high rejection rate is expected given the hydrogeology of the study site. The majority of rejected data are situated in the high salinity groundwater, prohibiting mobilization of ions necessary for polarization, leading to a low signal-to-noise ratio.

The difference between the normal and reciprocal profile is better illustrated by the apparent resistivity and chargeability plots (Fig. 3) where for each quadrupole the reciprocal is plotted in terms of the normal. In theory, the points should plot on the 1/1 line if the system behaves linearly. The apparent resistivity has a near-perfect fit with values between 0.0001 and 350 Ωm, and minimal outliers. The case is different for the apparent chargeability where a significant amount of the data has extreme values in the reciprocal profile (up to 1000 mV/V), this trend is also present in the normal but not as pronounced. Normal and reciprocal data are filtered independently, the non-linearity is hence still present in points retained for inversion and can be seen as a cluster of points on the horizontal and vertical axis.

The decay curves shown in Figure 4 shed more light on this deviation. The first column shows points where both curves have been accepted by the filtering procedure and hence retained for inversion, accounting for 31.71 % of the data. In some cases they have a perfect fit (e.g. Fig. 4a),

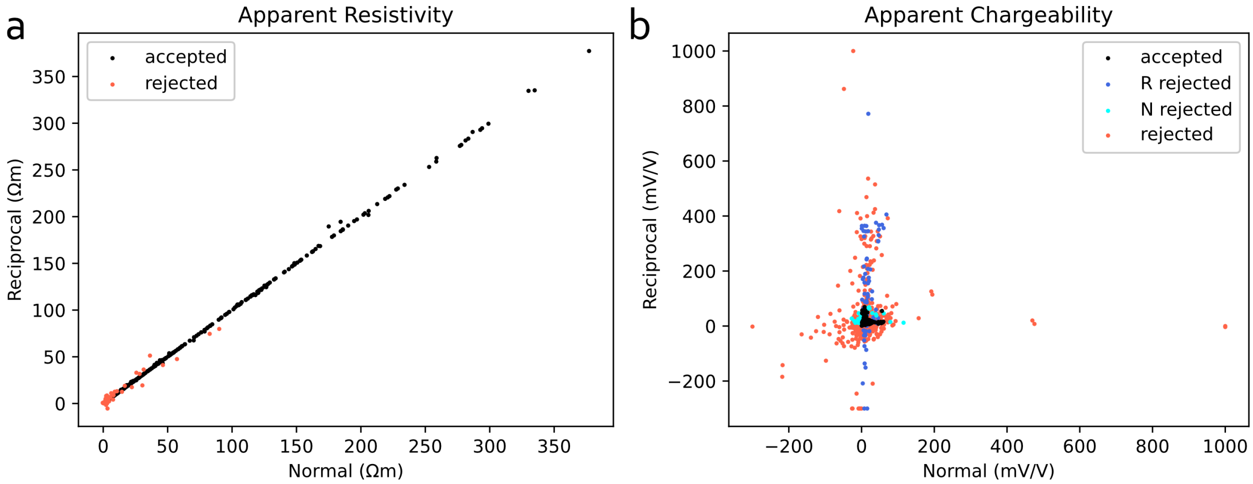

Figure 3. Normal-Reciprocal relationship for the a) apparent resistivity and b) apparent chargeability. Note that the data shown is unprocessed and includes erroneous measurements. For the chargeability rejected points are subdivided whether or not they are rejected in the normal, the reciprocal or both.

in other cases there is a shift between the two where either the normal curve is situated above the reciprocal (Fig. 4b,c) or vice versa (Fig. 4d,e). Column 2 contains points where the normal was retained and the reciprocal rejected, which is the case in 6.03 % of the data. In some cases, reciprocals are rejected because they are increasing instead of decaying (Fig. 4f), this so called negative IP effect arises from the sensitivity distribution associated with the measurement protocol (Dahlin & Zhou, 2004) and is only observed in the most shallow layer. In most cases, the reciprocal curves decay towards a non-zero value and were thus removed from the dataset. In these cases, the reciprocal has a clean decaying character but with a large shift in values compared to the normal of up to 250 mV/V. Column 3 shows the reverse situation, i.e. where the normal was rejected and the reciprocal retained for inversion, accounting for 5.04 % of the data. We might expect the reverse behavior as well but it is not the case, as the normal curves are simply rejected due to their noisy decay. Only in some cases, there is a shift between normal and reciprocal (e.g. Fig. 4k, l) but they do not have the significant deviation as the previous example. In the remaining 57.20 %, the data was removed for both the normal and reciprocal (Fig. 4p-t).

The apparent chargeability of the remaining dataset was transformed to phase shift φ using a constant phase angle model leading to conversion factor of -1.4 corresponding to the injection and measurement characteristics (Kemna, 2000; Thibaut et al., 2021). The inverted models are shown

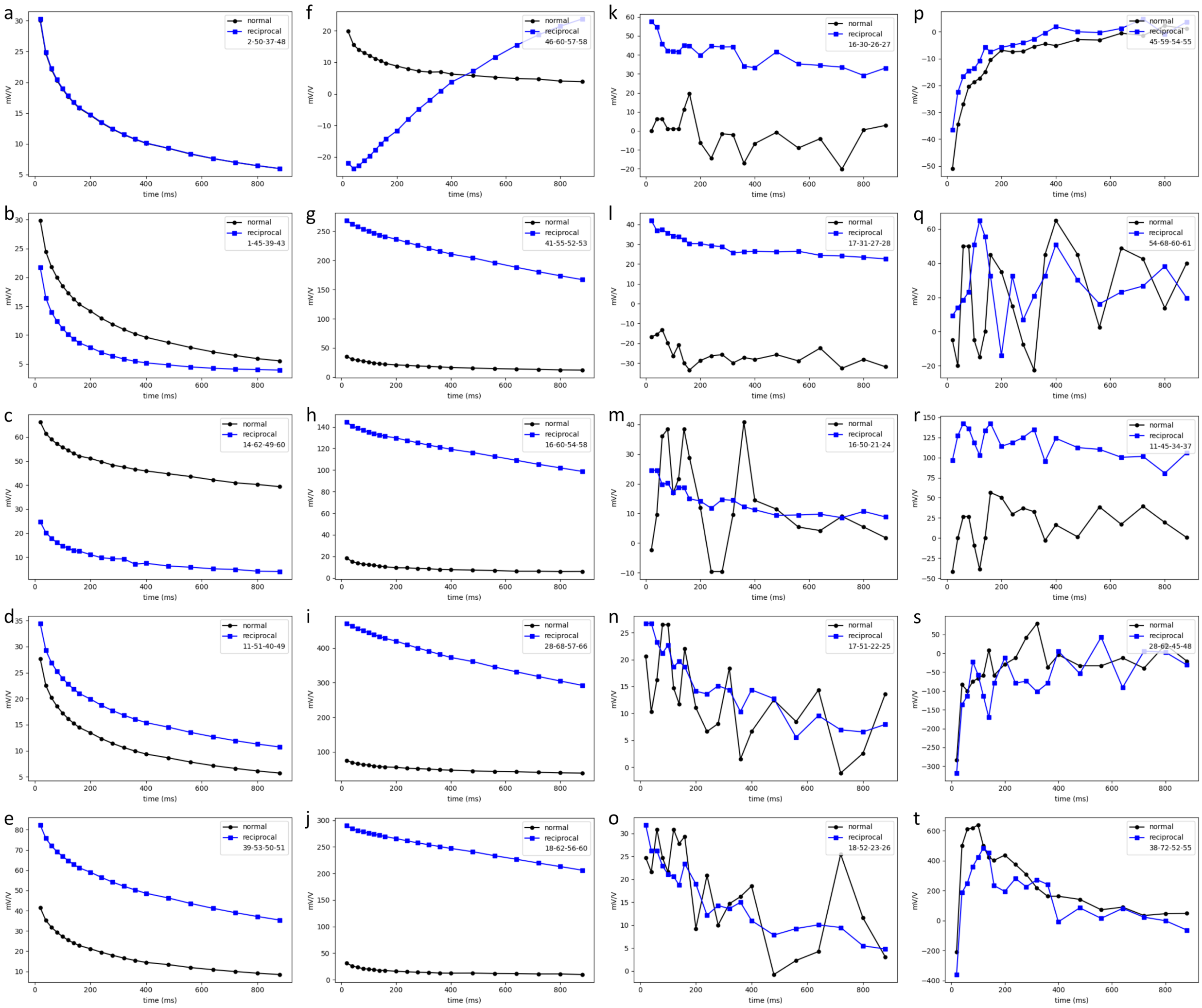

Figure 4. Normal and reciprocal decay curves of the same quadrupole. Column 1 (a-e) shows data that was retained for inversion in both normal and reciprocal. Column 2 (f-j) are cases where the normal was accepted and the reciprocal rejected. Column 3 (k-o), where the reciprocal was accepted and the normal rejected and column 4 (p-t), where both curves are rejected. The corresponding quadrupole is indicated as A-B-M-N.

in Figure 5, the complex conductivity is shown with its real and imaginary parts. In both the normal and reciprocal, the real conductivity is low (<300 mS/m) in the upper 10 m with a thicker anomaly between 180 and 300 m on the profile. For the real parameter, no observable difference is present between the normal and reciprocal, which is in line with the scatterplot of apparent resistivity (Fig. 3) knowing that $\sigma' = |\sigma| cos(-1.4) \approx |\sigma|$ (Binley & Slater, 2020). No indication of non-linear effects is therefore present. In the imaginary conductivity, two anomalies are present, the first one between 0 and 180 m, the second between 250 and 355 m with a plume-like geometry. Here, a

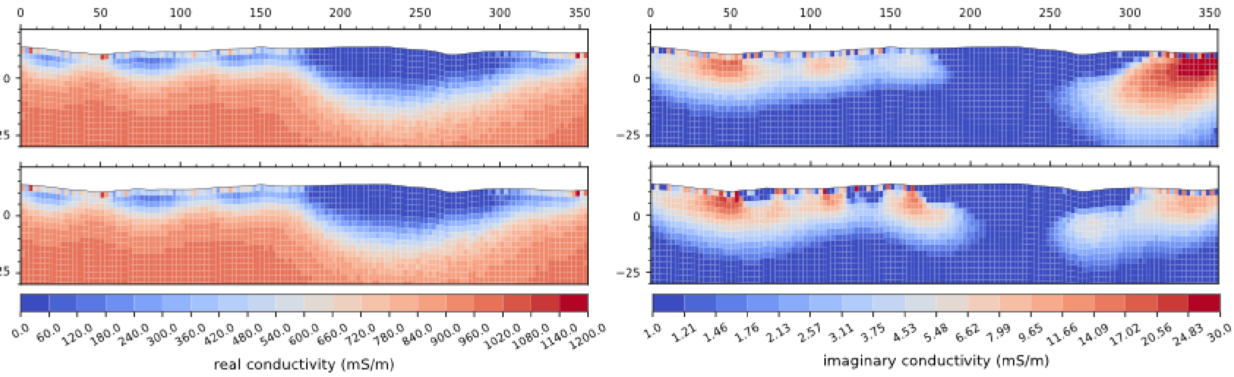

Figure 5. Inversions of the normal and reciprocal profile, the imaginary part of the conductivity has a significant difference in anomaly on the south side of the profile. The real part has no notable difference between the normal and reciprocal.

notable difference is resolved between the normal and reciprocal inversion, most strikingly in the second anomaly, which has values between 10-30 mS/m in the normal inversion but reaching only maximum 10 mS/m in the reciprocal inversion. The extent of the anomaly is similar in both cases, with some geometrical differences. In the normal inversion, it has a solid plume going downwards in shape, while in the reciprocal inversion, it is more patchy with a flattening of the plume around 10m depth. Differences between the normal and reciprocal are also present in the first anomaly, specifically in the area between 150-180 m. Here, the anomaly has lower values in the normal, up to 7 mS/m vs 15 mS/m in the reciprocal. Thus, here we observe a significant difference in the normal and reciprocal inversions, likely originating from the strong discrepancies between the measured apparent chargeability. This is better illustrated by the absolute difference of σ'' between normal and reciprocal (Fig. 6). The difference clearly indicates the previously described plume shape, with differences of 10-20 mS/m between normal and reciprocal, whilst discrepancies between 0-180 m are minor. As the difference is not observed everywhere along the profile, we can therefore exclude an origin only linked to the used protocols or the acquisition parameters. Because the data is acquired using a multigradient protocol, normal and reciprocal measurements correspond to different current densities. Following the reasoning of (Hallbauer-Zadorozhnaya et al., 2016), we interpret the difference as an indication of a non-linear IP effect.

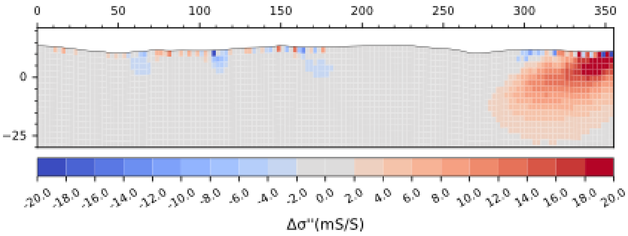

Figure 6. Absolute difference of the imaginary conductivity between the normal and reciprocal profile.

3.2 Stability of the non-linear IP effect

We hypothesise non-linear IP signals on the basis that the reciprocity theorem is not fulfilled. To ensure that the difference between the normal and reciprocal imaginary conductivity images (Fig. 6) is not the result of measurement errors, the analysis is repeated on the first 100 days of the monitoring campaign. If the results are consistent with the reference day, it indicates that the observed discrepancies are systematically observed within the data set.

Figure 7 shows the N/R mismatch trough time, the value of each point represents how many times it was rejected in the analysis. There are two clusters of points with a high mismatch rate (90-100 %); between 220-355 m, corresponding to the strong nonlinear IP response and between 100-150m, where the mismatch rate is lower (80-90 %). Figure 9 shows a scatterplot of the apparent chargeability of two monitoring days, 20 days apart, confirming consistency through time. When the normal values are grouped between 0 and 200 mV/V, the same is true for the reciprocal but with a cluster reaching 1000 mV/V but remaining on the 1/1 line.

Figure 8 is the timelapse equivalent of Figure 4, columns 2 and 3 concern data with a high mismatch rate between normal and reciprocal (<80 %). In cases where the normal is accepted and the reciprocal rejected (Fig. 8f-j), rejects happened mainly because of decay towards a positive value, which is consistent throughout time. A shift of <100mV/V is present between normal and reciprocal, while the reciprocal itself remains of good quality. It is striking that the values of the reciprocal decay curves are widely spread (100-200 mV/V difference) while the normal decay curves are spread over a much smaller interval (max 40 mV/V) and are hence more stable through time. Disregarding the fact that the reciprocal decay curves have a wide range of values, a considerable shift is still present in most cases. In the opposite case, when the normal is rejected and

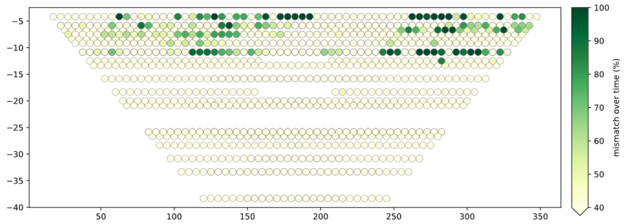

Figure 7. Pseudosection showing how many times each quadrupole has been flagged as having a mismatch between the normal and reciprocal

the reciprocal accepted (Fig. 8k-o), the main reason for the mismatch was the poor quality of the normal rather than a shift between the curves, which is consistent throughout time as well. A big spread in the values between the decay curves is not inherent to the reciprocal, but is also observed in the normal profile (Fig. 8c), in cases where the data is accepted in both profiles the curves do not always match perfectly as is the case in (Fig. 8a), but can exhibit a spread for both the normal and reciprocal.

Inversion of the filtered datasets at subsequent dates was done using the same inversion parameters; the absolute change in imaginary conductivity is calculated with the first day as a reference (Fig. 10). Only the imaginary part is shown here, as this is where the anomaly is observed. The first two timelapse images of the normal profile have minor changes at the surface in the area with the anomaly, from 12-13-2022 onward, stronger changes are present, in the range of 5 mS/m, as the change remains constant, it likely points to a change in the system. In the reciprocal no significant changes are observed. Hence we can state that the IP anomaly remains relatively stable in both cases. Since the observed changes through time are lower than the difference between the normal and reciprocal inversions of the initial profile (Fig. 6), we conclude that the difference between normal and reciprocal data cannot be explained by a variability of the signal related to noise, but its explanation is rooted in the non-linear effect.

It should be noted that Fig. 10 is based on the difference of two absolute inversions, which is known to be prone to artefacts of inversion (Kemna, 2000; Singha et al., 2015). A real time-lapse inversion, using, for example, the difference inversion scheme would focus the inversion on the change in the signal change and would likely limit further the presence of artefacts but this is out of the scope of this study.

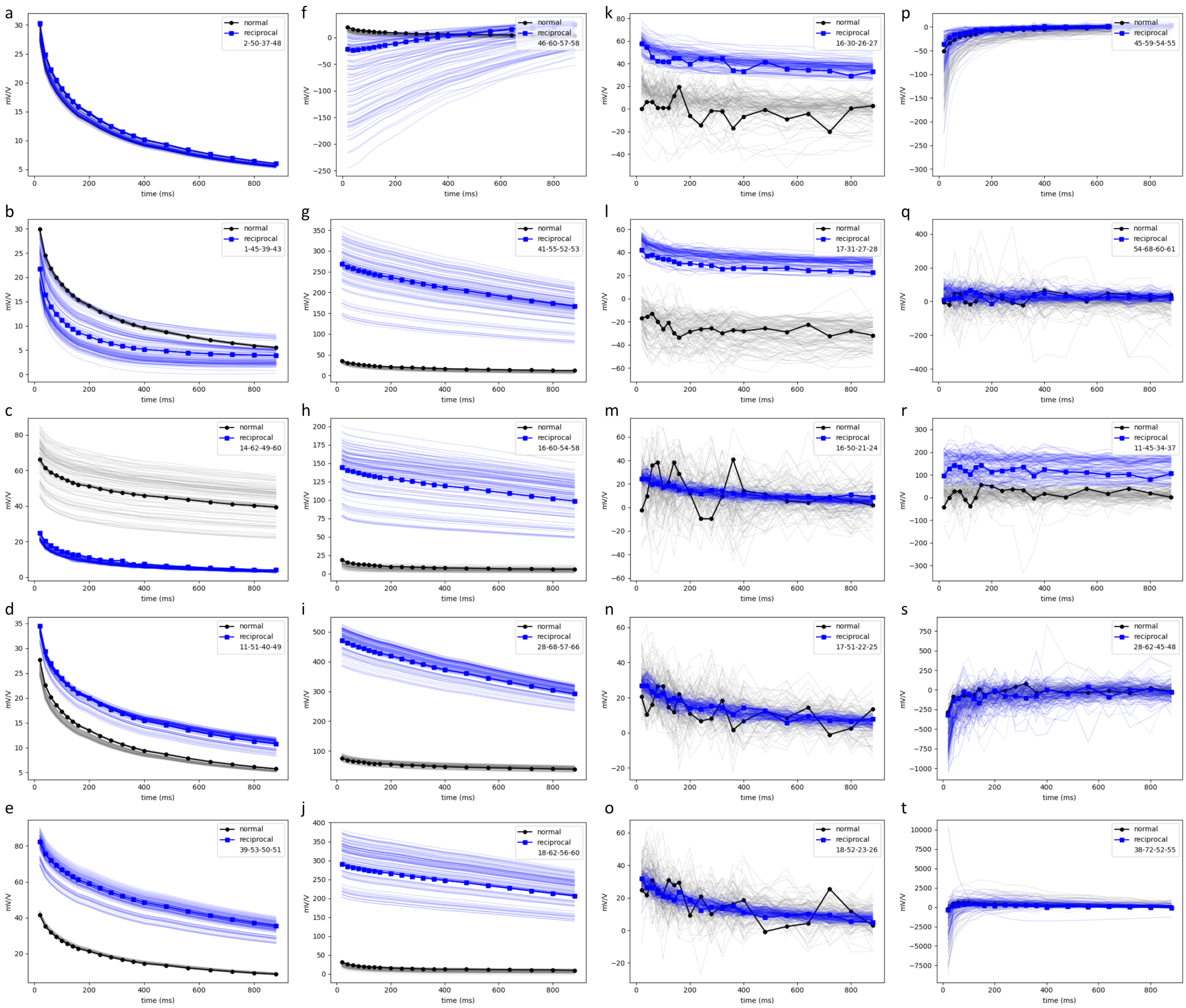

Figure 8. Decay curves of the 100 analyzed dates, the quadrupoles correspond to the ones shown in Fig. 4 with the muted lines representing the subsequent measurements.

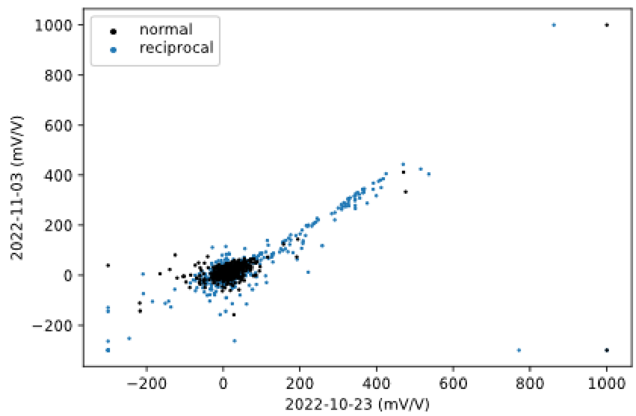

Figure 9. Apparent chargeability of two days for the normal and reciprocal. The reference day (2022-10-23) is plotted against one of the monitoring days (2022-11-03). Note that this concerns raw data.

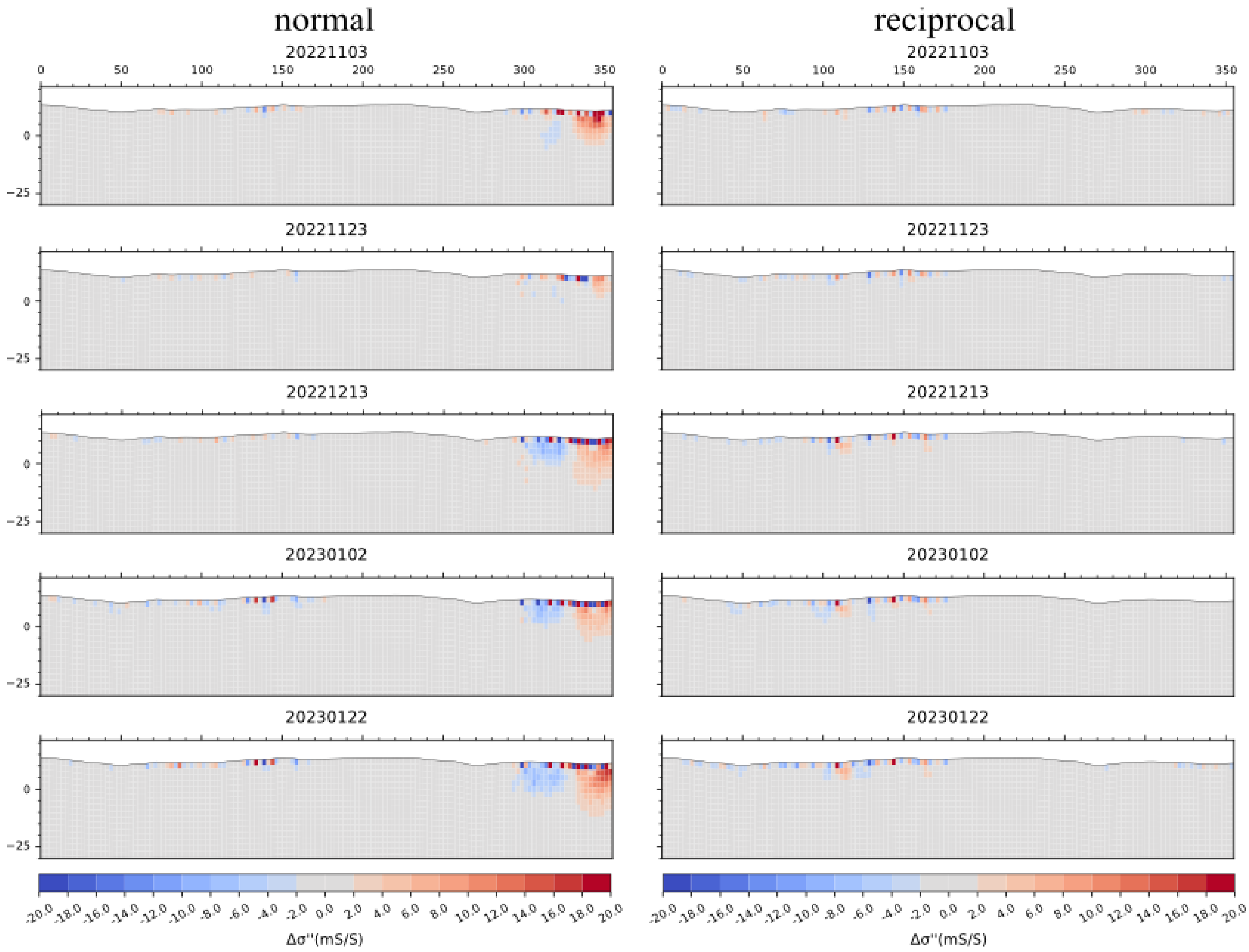

Figure 10. Timelapse images of the imaginary conductivity in both the normal and reciprocal settings. The reference day is 2022-10-23, a timelapse image is shown every 20 days.

3.3 Discussion

In the polarizable part of the signal, a strong discrepancy is observed between normal and reciprocal which is consistent trough time. In the data this is discernible as a cluster of points with a higher chargeabilitiy in the reciprocal, reflected as well by the decay curves where a positive shift is present of up to 200 mV/V. In the inverted models, the anomaly in the imaginary part of the conductivity, σ'', is stronger in the normal compared to the reciprocal, the opposite of what might be expected from the data. This can be attributed to the filtering procedure, decay curves that do not decay towards zero are removed from the dataset, including curves that decay towards a positive value. If these curves would be maintained and incorporated in the inversion, the integral chargeability would be extremely high (few 100 mV/V), hence it is expected that the anomaly would be stronger instead of weaker. Including this however, would introduce ambiguities in the interpretation. If the point was allowed to fully decay, the remainder of the curve (or tail) would encompass a significant portion of the signal, hence, the integral chargeability will be systematically underestimated. This clearly illustrates the complex nature of non-linear signals, neither inversion can reflect the actual distribution of the property in the subsurface as is inherent to non-linearity. Hence, we suggest the presence of such signals should rather be used as a qualitative interpretation tool.

No significant difference is observed in the non-polarizable part of the signal, and can be attributed to a scaling effect rather than the linear behaviour of the real part of the conductivity. Since the imaginary part is several orders of magnitude smaller than the real part of the conductivity, these subtle differences are more discernible.

We used time-lapse data to prove that the discrepancy between normal and reciprocal data is consistent through time. The inversion showed that some permanent variations are observed when inverting the normal data sets, while none are observed in the reciprocal data. It is difficult to interpret if these small changes could be linked to actual variations on the field. The system is hydrothermally active and changing constantly, but it is unclear if the period reported in this paper is sufficient to explain permanent change in imaginary conductivity. If it were the case, it seems however that this changes could be also related to a non-linear effect as they are not imaged in the reciprocal profile.

Given the geological context of the data presented here, we hypothesize that the non-linear signal is likely linked to oxidation-reduction of iron containing minerals which would correspond with a strong IP signal in the static images, as is the case here. The presence of sulfides in samples collected on the field has been confirmed while Vanhooren et al. (2025) found strong self potential anomalies in the area where the discrepancy between normal and reciprocal data is observed, confirming that oxido-reduction processes are a valid explanation for the observed behaviour. Hallbauer-Zadorozhnaya et al. (2015) additionally found evidence for non-linearity in the non-polarize part, which is not the case in our data, but this could be linked to the conductive nature of the field. Additional field investigations are needed to confirm this hypothesis.

4 CONCLUSION

In this contribution, the normal and reciprocal measurements of a TDIP profile were processed independently of each other, allowing us to invalidate the linearity assumption of the reciprocity theorem. The reciprocity theorem states that given a linear response, interchanging the potential and current electrodes should yield the same results (Parasnis, 1988). In the Reykjanes dataset, the linearity principle holds for the resistivity parameter, there is a nearly perfect match for the apparent resistivity and the real conductivity σ' model has no observable differences. In the polarizable part, however, there is a clear difference; there is a cluster of points where the apparent chargeability is significantly higher in the reciprocal, corresponding to curves that decay towards a positive value but otherwise exhibit a clean decaying trend. Data such as these are removed after decay curve analysis because they introduce an extra level of ambiguity. The inverted model has a plume-like anomaly in the imaginary conductivity σ'' that is significantly stronger in the normal profile with a deviation of up 20 mS/m. The deviation is mainly caused by the shift in normalized chargeability, these curves could be related to polarization at the electrode. However, since the deviation is localized, the signal is related to a natural phenomenon rather than poor survey design. In order to eliminate a noise or measurement error-related cause, the analysis was done for 100 consecutive days and showed consistent results, the anomaly of the imaginary conductivity is stable in the reciprocal profile and displays small changes in the normal that remain stable so are more likely related to a change of the system. Moreover, the variation of the normal profile is smaller than the absolute difference between the normal and reciprocal. The dataset is part of a continuous ERT/TDIP experiment on the Reykjanes geothermal area in Iceland, the field is prone to strong alterations and other geothermal expressions. In this context, the non-linear IP signal is likely related to oxidation-reduction reactions of iron oxides such as pyrite. The signal is present in an area of the profile without corresponding surface alterations, we hypothesise that the shallow precipitation of minerals forms a seal prohibiting hydrothermal fluids from reaching the surface and causing progressive alteration. The reciprocal profile is widely used in geo-electric surveys but mainly from a data-quality perspective here we argue for an additional purpose as an interpretation tool. An additional advantage is that the method does not require advanced modelling techniques or the measurement of spectral data, making it suitable and easy to use for field surveys.

References

Archie, G. E., 1941. The electrical resistivity log as an aid in determining some reservoir characteristics, *Transactions AIME*, pp. 54–62.

Binley, A. & Slater, L., 2020. *Resistivity and Induced Polarization - Theory and Applications to the Near-Surface Earth*, cambridge university press.

Björnsson, S., Arnorsson, S., & Tomasson, J., 1970. Exploration of the reykianes thermal brine area, *Geothermics*, **2**, 1640–1650.

Bretaudeau, F., Dubois, F., Kassa, S. G. B., Coppo, N., Wawrzyniak, P., & Darnet, M., 2021. Time-lapse resistivity imaging: Csem-data 3-d double-difference inversion and application to the reykjanes geothermal field, *Geophysical Journal International*, **226**, 1764–1782.

Caterina, D., Hermans, T., & Nguyen, F., 2014. Case studies of incorporation of prior information in electrical resistivity tomography: Comparison of different approaches, *Near Surface Geophysics*, **12**, 451–465.

Dahlin, T. & Zhou, B., 2004. A numerical comparison of 2d resistivity imaging with 10 electrode arrays, *Geophysical Prospecting*, **52**, 379–398.

Defourny, A., Nguyen, F., Collignon, A., Jobé, P., Dassargues, A., & Kremer, T., 2020. Induced polarization as a proxy for co2-rich groundwater detection—evidences from the ardennes, south-east of belgium, *Water*, **12**(5).

Evrard, M., Dumont, G., Hermans, T., Chouteau, M., Francis, O., Pirard, E., & Nguyen, F., 2018. Geophysical investigation of the pb–zn deposit of lontzen–poppelsberg, belgium, *Minerals*, **8**.

Flores-Orozco, A., Williams, K. H., Long, P. E., Hubbard, S. S., & Kemna, A., 2011. Using complex resistivity imaging to infer biogeochemical processes associated with bioremediation of an uranium-contaminated aquifer, *Journal of Geophysical Research: Biogeosciences*, **116**.

Flores Orozco, A., Gallistl, J., Bücker, M., & Williams, K. H., 2018. Decay curve analysis for data error quantification in time-domain induced polarization imaging, *GEOPHYSICS*, **83**(2), E75–E86.

Fowler, A. P., Zierenberg, R. A., Schiffman, P., Marks, N., & omar Fridleifsson, G., 2015. Evolution of fluid-rock interaction in the reykjanes geothermal system, iceland: Evidence from iceland deep drilling project core rn-17b, *Journal of Volcanology and Geothermal Research*, **302**, 47–63.

Fridleifsson, G. O., Elders, W. A., Zierenberg, R. A., Fowler, A. P., Weisenberger, T. B., Mesfin, K. G., Sigurdsson, O., Níelsson, S., Einarsson, G., Oskarsson, F., Gudnason, E., Tulinius, H., Hokstad, K., Benoit, G., Nono, F., Loggia, D., Parat, F., Cichy, S. B., Escobedo, D., & Mainprice, D., 2020. The iceland deep drilling project at reykjanes: Drilling into the root zone of a black smoker analog, *Journal of Volcanology and Geothermal Research*, **391**, 106435.

Fridriksson, T., Kristjánsson, B. R., Ármannsson, H., Margrétardóttir, E., Ólafsdóttir, S., & Chiodini, G., 2006. Co2 emissions and heat flow through soil, fumaroles, and steam heated mud pools at the reykjanes geothermal area, sw iceland, *Applied Geochemistry*, **21**, 1551–1569.

Ghorbani, A., Revil, A., Coperey, A., Ahmed, A. S., Roque, S., Heap, M. J., Grandis, H., & Viveiros, F., 2018. Complex conductivity of volcanic rocks and the geophysical mapping of alteration in volcanoes, *Journal of Volcanology and Geothermal Research*, **357**, 106–127.

Hallbauer-Zadorozhnaya, V., Santarato, G., & Abu Zeid, N., 2015. Non-linear behaviour of electrical parameters in porous, water-saturated rocks: a model to predict pore size distribution, *Geophysical Journal International*, **202**(2), 871–886.

Hallbauer-Zadorozhnaya, V. Y., Santarato, G., Zeid, N. A., & Bignardi, S., 2016. A non-linear induced polarization effect on transient electromagnetic soundings, *Journal of Applied Geophysics*, **133**, 16–24.

Hermans, T. J., 2014. *Integration of near-surface geophysical, geological and hydrogeological data with multiple-point geostatistics in alluvial aquifers*.

Kadko, D., Gronvold, K., & Butterfield, D., 2007. Application of radium isotopes to determine crustal residence times of hydrothermal fluids from two sites on the reykjanes peninsula, iceland, *Geochimica et Cosmochimica Acta*, **71**, 6019–6029.

Karlsdottir, R., Vilhjálmsson, A. M., & Árni Gudnason, E., 2020. Three dimensional inversion of magnetotelluric (mt) resistivity data from reykjanes high temperature field in sw iceland, *Journal of Volcanology and Geothermal Research*, **391**.

Kemna, A., 2000. *Tomographic inversion of complex resisitvity-theory and application.*.

Lesmes, D. P. & Frye, K. M., 2001. Influence of pore fluid chemistry on the complex conductivity and induced polarization responses of berea sandstone, *Journal of Geophysical Research: Solid Earth*, **106**(B3), 4079–4090.

Lévy, L., Gibert, B., Sigmundsson, F., Flóvenz, O. G., Hersir, G. P., Briole, P., & Pezard, P. A., 2018. The role of smectites in the electrical conductivity of active hydrothermal systems: Electrical properties of core samples from krafla volcano, iceland, *Geophysical Journal International*, **215**, 1558–1582.

Lévy, L., Maurya, P. K., Byrdina, S., Vandemeulebrouck, J., Sigmundsson, F., Árnason, K., Ricci, T., Deldicque, D., Roger, M., Gibert, B., & Labazuy, P., 2019. Electrical resistivity tomography and time-domain induced polarization field investigations of geothermal areas at krafla, iceland: Comparison to borehole and laboratory frequency-domain electrical observations, *Geophysical Journal International*, **218**, 1469–1489.

Marks, N., Schiffman, P., Zierenberg, R. A., Franzson, H., & o Fridleifsson, G., 2010. Hydrothermal alteration in the reykjanes geothermal system: Insights from iceland deep drilling program well rn-17, *Journal of Volcanology and Geothermal Research*, **189**, 172–190.

Oldenburg, D. W. & Li, Y., 1994. Subspace linear inverse method, *Inverse Problems*, **10**, 915–935.

Olhoeft, G., 1979. Nonlinear electrical properties, *Nonlinear behavior of molecules, atoms and ions in electric, magnetic or electromagnetic fields, Neel, L.(ed.), Elsevier Publishing Co., Amsterdam*, pp. 395–410.

Olhoeft, G., 1985. Low-frequency electrical properties, *Geophysics*, **50**(12), 2492–2503.

Parasnis, D., 1988. Reciprocity theorems in geoelectric and geoelectromagnetic work, *Geoexploration*, **25**(3), 177–198.

Pelton, W. H., Wards, S. H., Hallof, P. G., Sills, W. R., & Nelson5, P. H., 1978. Mineral discrimination and removal of inductive coupling with multifrequency ip, *GEOPHYSICS*, **43**.

Revil, A., Hermitte, D., Spangenberg, E., & Cochemé, J. J., 2002. Electrical properties of zeolitized volcaniclastic materials, *Journal of Geophysical Research: Solid Earth*, **107**.

Sigurdsson, F., 1986. Hydrogeology and groundwater on the reykjanes peninsula, *Jökull*, **36**, 11–29.

Singha, K., Day-Lewis, F. D., Johnson, T., & Slater, L. D., 2015. Advances in interpretation of subsurface processes with time-lapse electrical imaging, *Hydrological Processes*, **29**(6), 1549–1576.

Slater, L., Binley, A., Daily, W., & Johnson, R., 2000. Cross-hole electrical imaging of a controlled saline tracer injection, *Journal of Applied Geophysics*, **44**, 85–102.

Slater, L. D. & Lesmes, D., 2002. Ip interpretation in environmental investigations, *Geophysics*, **67**(1), 77–88.

Slater, L. D., Choi, J., & Wu, Y., 2005. Electrical properties of iron-sand columns: Implications for induced polarization investigation and performance monitoring of iron-wall barriers, *Geophysics*, **70**(4), G87–G94.

Sæmundsson, K., Sigurgeirsson, M., & omar Fridleifsson, G., 2020. Geology and structure of the reykjanes volcanic system, iceland, *Journal of Volcanology and Geothermal Research*, **391**.

Thibaut, R., Kremer, T., Royen, A., Ngun, B. K., Nguyen, F., & Hermans, T., 2021. A new workflow to incorporate prior information in minimum gradient support (mgs) inversion of electrical resistivity and induced polarization data, *Journal of Applied Geophysics*, **187**.

Troiano, A., Isaia, R., Tramparulo, F., & Di Giuseppe, M., 2021. The pisciarelli main fumarole mechanisms reconstructed by electrical resistivity and induced polarization imaging, *Scientific Reports*, **11**(1), 18639.

Vanhooren, L., Vrancken, E., Dekoninck, W., Flores-Orozco, A., Fontaine, O., Bergursson, B., Jonsdottir, K., Caudron, C., & Hermans, T., 2025. *Volcanica*.

Waxman, M. H. & Smits, L., 1968. Electrical conductivities in oil-bearing shaly sands, *Society of Petroleum Engineers Journal*, **8**(02), 107–122.

Weller, A., Zhang, Z., & Slater, L., 2015. High-salinity polarization of sandstones, *GEO-*

PHYSICS, **80**(3), D309–D318.

Weller, A., Zhang, Z., Slater, L., Kruschwitz, S., & Halisch, M., 2016. Induced polarization and pore radius—a discussion, *Geophysics*, **81**(5), D519–D526.